A conserved copper-binding site in multicopper oxidases regulates the metalation of CueO from Escherichia coli

Paolo Santucci, Frédéric Biaso, Jérôme Becam, Ludovic Dubard, Marianne Ilbert, Benjamin Ezraty, Ievgen Mazurenko, Elisabeth Lojou, Umberto Contaldo

Journal of Inorganic Biochemistry 278 (2026) 113257

Contents lists available at ScienceDirect

Journal of Inorganic Biochemistry

journal homepage: www.elsevier.com/locate/jinorgbio

A conserved copper-binding site in multicopper oxidases regulates the metalation of CueO from *Escherichia coli*

Paolo Santucci [a], Frédéric Biaso [a], Jérôme Becam [b], Ludovic Dubard [a], Marianne Ilbert [a], Benjamin Ezraty [b], Ievgen Mazurenko [a], Elisabeth Lojou [a,*], Umberto Contaldo [a,*]

[a] Aix Marseille Univ., CNRS, Laboratoire de Bioénergétique et Ingénierie des Protéines (BIP), Institut de Microbiologie de la Méditerranée, 13402 Marseille, France
[b] Aix Marseille Univ., CNRS, Laboratoire de Chimie Bactérienne (LCB), Institut de Microbiologie de la Méditerranée, 13402 Marseille, France

ARTICLE INFO

Keywords:
Cuproxidase CueO
Metalation
Maturation
Copper homeostasis
Electrochemistry
Multicopper oxidase

ABSTRACT

CueOs are multicopper oxidases (MCOs) involved in key biological processes related to copper homeostasis. Their physiological function is the catalytic oxidation of toxic cuprous ions (Cu^{+}) to cupric ions (Cu^{2+}), coupled with the reduction of O_2 to water. In addition to the copper sites belonging to the classical electron transfer chain of MCOs, from Cu-T1 to the trinuclear cluster (TNC), a Cu8-site was previously identified in *Ec*CueO crystal structures, located in close proximity to TNC. One conserved ligand of the Cu8-site is the amino acid H_{145}, in both Cu^{+} and Cu^{2+} redox states. By designing and characterizing the $H_{145}S$ variant, this work demonstrates for the first time the pivotal role of H_{145} in the functional maturation/metalation of *Ec*CueO active sites under conditions of low Cu^{2+}/Cu^{+} availability. Moreover, we show that H_{145} is part of a conserved HxHxH motif in CueOs, and more generally in bacterial MCOs, suggesting a common copper-binding Cu8-site for metalation *in vivo*. The absence of this conserved motif in certain MCOs, or the presence of additional His/Met-rich or His-rich insertions, appears to be linked to cellular copper availability and highlights the adaptability of MCOs. Beyond this fundamental understanding of MCO metalation mechanism, this works paves the way for application in medicine and environmental copper detection.

1. Introduction

The multicopper oxidase (MCO) superfamily is distributed extensively throughout nature, with members present in organisms ranging from archaea to animals, including humans [1–7]. MCOs are defined by the presence of a highly conserved protein architecture composed of repeated cupredoxin domains, ranging from a minimum of two (2dMCO) to three (3dMCO) and up to six domains (6dMCO). This structural arrangement facilitates the coordination of the protein cofactors: the mononuclear Cu-T1 and a trinuclear cluster (TNC), comprising one Cu-T2 and a binuclear Cu-T3. The Cu-T1 is responsible for the oxidation of various substrates, including, but not limited to, mono- and polyphenols, metal ions, diamine, biogenic amines, or epoxy-based polymers [8–13]. The generated electrons are transferred to the TNC, which catalyzes the concomitant four-electron reduction of O_2 to H_2O (Oxygen Reduction Reaction, ORR), making MCOs attractive enzymes for use in bio-electrochemical devices. The 3dMCO CueO subfamily is distinguished by an additional partially disordered domain that is enriched in histidine and methionine residues (His/Met-rich). The His/Met-rich region demonstrates high variability in size according to the microbiological source [3]. Furthermore, most of this domain is predicted to adopt a random coil conformation and remains unresolved in crystallographic structures [14–22]. The analysis of *Escherichia coli* CueO (*Ec*CueO) crystallographic structures obtained in presence of an excess of copper [14,23], revealed the coordination of the standard MCO cofactors (Cu-T1, Cu-T2, Cu-T3) and additional copper atoms, including Cu5, Cu6, Cu7 and Cu8, according to the nomenclature used by Contaldo et al. [24] (**Fig. S1**). CueOs are periplasmic enzymes involved in

Abbreviations: (Cu^{+}), Cuprous; (Cu^{2+}), Cupric; (MCOs), Multicopper oxidases; (His), Histidine; (Met), Methionine; *(Ec)*, *Escherichia coli*; (TNC), Trinuclear cluster; (ORR), Oxygen Reduction Reaction; (DET), Direct electron transfer; (CNT), Carbon nanotube; (WT), Wild-type; (APO), Copper free; (HOLO), Copper loaded; (Å), Angströms; (PCR), Polymerase reaction chain; (OD), Optical density; (PBS), Phosphate buffer saline; (EPR), Electron Paramagnetic Resonance; (ABTS), 2,2′-azino-bis (3-ethylbenzothiazoline-6-sulfonic acid); (BCA), Bicinchoninic acid disodium salt hydrate; (CV), Cyclic voltammetry; (CA), Chronoamperometry; (NHE), Normal Hydrogen Electrode; (ω), Rotation speed; (LAB), Lactic acid bacteria; ($V_{max}/_{app}K_m$), Catalytic efficiency.

* Corresponding authors.
E-mail addresses: lojou@imm.cnrs.fr (E. Lojou), ucontaldo@imm.cnrs.fr (U. Contaldo).

https://doi.org/10.1016/j.jinorgbio.2026.113257
Received 9 December 2025; Received in revised form 17 January 2026; Accepted 4 February 2026
Available online 5 February 2026

copper homeostasis by catalyzing the oxidation of Cu^{+} to the less toxic Cu^{2+}, which constitutes their native activity [25,26]. We recently demonstrated that Cu6 and Cu7 do not participate directly in cuprous oxidation [24]. Instead, these two Cu^{+}-binding sites likely represent the pathway of Cu^{+} recruitment facilitating the oxidation of cuprous ions. We showed that the oxidation of Cu^{+} in CueO enzymes is catalyzed by Cu5-site which is found in close proximity to the Cu-T1, thus transferring electrons to Cu-T1, to TNC and then to O_2 [24,27]. Among the other additional copper sites, Cu8 stands out as it has been consistently observed in two related structural studies, first reported in 2011 by Singh et al. [23] and later confirmed in 2018 by Wang et al. [14]. In the 2011 study, Cu8, in the reduced Cu^{+} state, was found to be coordinated by H_{145}, M_{417}, and two water molecules (Fig. 1). In the 2018 study, Cu8, in the oxidized Cu^{2+} state, was still coordinated by H_{145}, but also by one water molecule and H_{406} (Fig. 1). Regardless of the redox state of the Cu8, the coordination by H_{145} is conserved in both structures and is positioned at an average distance of 13–14 Å from one Cu-T3, potentially enabling electron transfer. It is noteworthy that H_{145} constitutes part of a protein loop and is located downstream the sequence of H_{141} and H_{143}, which are ligands for the two Cu-T3.

Catalysis by MCOs has been widely exploited with the protein immobilized on electrodes in view of ORR in bioelectrochemical applications, including dioxygen biosensors and enzymatic fuel cells [28,29]. The establishment of electrical contact between the electrode and the protein's first electron acceptor, Cu-T1, enables the enzymatic catalysis through direct electron transfer (DET). We previously examined the impact of Cu^{2+} ions on the DET-type ORR by *Ec*CueO immobilized on carbon nanotube (CNT) functionalized electrode [30]. We showed that in the presence of millimolar Cu^{2+}, a decrease in the DET current at low potentials was observed associated with enzyme inactivation and subsequent reactivation processes (Cu-RI). Recent electrochemical data obtained in the group of K. Sowa demonstrated that H_{145}, a residue that they showed to be conserved in three different MCOs, is the main Cu8 ligand that induces the Cu-RI [31]. Besides, we recently proposed the *in situ* metalation of APO CueOs assisted by electrochemistry [32]. In the presence of nanomolar concentrations of Cu^{2+}, and following the electrogeneration of Cu^{+} ions at low potentials, the ORR by *Ec*CueOs immobilized at electrodes progressively increased before reaching a steady-state. The activated current persisted after the bioelectrode was transferred to a copper free solution, indicating that the activation process was not related to Cu^{+}-oxidase activity. The electro-assisted *in situ* metalation process was found to be independent of both the His/Met-rich domain and the Cu5-site, and was hypothesized to be driven by copper coordination at one of the additional copper binding sites

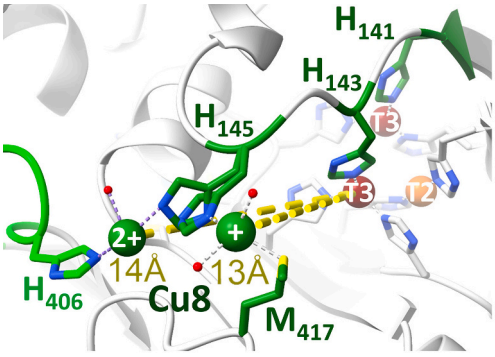

Fig. 1. Ribbon diagram of *E. coli* CueO X-ray structures (PDB entries: 3OD3, 3NT0, 5YS5). Copper atoms represented as spheres with van der Waals radii of 1.5 Å. H_{141}, H_{143} and H_{145} residues belong to a protein loop that provides one ligand for each Cu-T3 and one for the Cu8. An adjacent loop provides the M_{417} that represents the second Cu8 ligand for the Cu^{+} state. The His/Met-rich domain (lime green) provides the H_{406} that represents the second Cu8 ligand for the Cu^{2+} redox state. (For interpretation of the references to colour in this figure legend, the reader is referred to the web version of this article.)

present in *Ec*CueO, which we could not identify at that time. Given its position in close proximity to Cu-T3 and its conservation across MCOs, we examined here whether H_{145}, as well as Cu8-site, could play a key role in the metalation of CueO.

Hence, in the current work, we present original results obtained with an *Ec*CueO variant in which H_{145} was substituted by a serine ($H_{145}S$). Preliminary, an in-silico analysis highlights that the H_{145} belongs to a conserved HxHx(H/C/M) motif frequently exhibited in bacterial MCOs structures. An exhaustive comparison of $H_{145}S$ activity with *Ec*CueO wild-type (WT) one was undertaken in solution and once the enzymes are immobilized at electrochemical interfaces using complementary biochemical and physicochemical methods. Starting from copper free (APO) enzymes, this work demonstrates that H_{145} plays a critical role in the proper *in vitro* maturation and metalation of *Ec*CueO. Our work especially highlights that the presence of H_{145} facilitates APO *Ec*CueO in detecting traces of Cu^{+}/Cu^{2+}, thereby enabling enzyme metalation even in conditions of extremely low copper availability. Finally, given the conservation of the HxHx(H/C/M) motifs in many MCOs, its lacks or presence of additional His/Met-rich insertions in some others, we discuss in this work the modulation of the function of Cu8 depending on the cellular environment.

2. Material and methods

2.1. Protein modelling and structural analysis of Cu8 ligands

Molecular visualization and structural analysis were carried out using UCSF ChimeraX 1.10.1 (University of California, USA) [34,35]. The crystallographic structures of *Ec*CueOs were obtained from PDB entries 3OD3, 3NT0 and 5YS5, for the full-length resolved, Cu^{+}-bound and Cu^{2+}-bound, respectively. In Fig. 1 and **Fig. S1** the protein backbone is illustrated as a ribbon model, with the His/Met-rich domain colored in lime green and the remaining region in light gray. To enhance clarity, copper atoms are shown as spheres with a van der Waals radius of 2.0 angströms (Å). Copper-coordinating residues are depicted as stick representations. Atom distances in Å are highlighted by colored dashed lines in Fig. 1 and **Fig. S1**.

For the identification of the degree of Cu8 ligands conservation among MCO enzymes, an initial screening of the available crystallographic structure results in the selection of various MCOs (**Table S3**). The structure-based alignment of each selected MCO in comparison to *Ec*CueO Cu8-site is provided in the supporting information (**Fig. S2**, **Fig. S3**, **Fig. S4**, **Fig. S5**, **Fig. S6**).

2.2. Plasmid construction

The plasmids used in this study are listed in **Table S1**. The plasmid pJB313 was constructed by amplifying the plasmid pAV97 using primers JB605 and JB606 (**Table S2**) that allow insertion of the mutation $H_{145}S$. The primers JB605 and JB606 were used to amplify the backbone vector pAV97, allowing complementary ends. Finally, the plasmid pJB313 was obtained by ligation of the polymerase reaction chain (PCR) fragment with 5× InFusion Snap assembly kit following supplier recommendations. The plasmid pJB313 was sequenced to verify the construction.

2.3. Copper-free (APO) EcCueO expression and purification

The medium used for the expression of APO *Ec*CueO was LB Broth (Miller's) with 100 μg mL^{-1} ampicillin. This medium contains less than 0.01 μM copper as determined by ICP-OES. *E. coli* cells containing the desired plasmid were cultivated at 37 °C until an optical density (OD) at 600 nm of 0.6–0.8 was attained. Thereafter, 0.1 mM IPTG was incorporated to induce gene expression, and the cells were maintained at 25 °C for a duration of 24 h, reaching an $OD_{600\ nm}$ of 5–6. The cells were harvested by means of centrifugation at 5000 rpm, after which they were washed with 50 mM saline phosphate buffer (PBS) at pH 7.4.

Bacteria pellets were resuspended at 4 °C in 50 mM PBS at pH 7.4, containing a protease inhibitor cocktail, 10 μg mL^{-1} DNase I and 2 mM $MgSO_4$. Cell lysis was performed using a French Press (Thermo Scientific) at 4 °C, 1000 psi, for two cycles. The removal of cell debris was achieved through ultracentrifugation at a speed of 40,000 rpm for a duration of 45 min at a temperature of 4 °C. The cleared lysate was subjected to filtration using a 0.45 μm filter prior to loading onto a 5 mL Strep-Tactin®XT 4Flow® (IBA Lifesciences) column. Non-adsorbed proteins were subsequently washed with 50 mM PBS at pH 7.4 with 150 mM NaCl. Adsorbed *Ec*CueOs were then eluted with 50 mM PBS at pH 7.4 with 5 mM biotin. Eluted colorless *Ec*CueOs were concentrated up to 100 μM and desalted with 40 mM MOPS buffer at pH 7.0, using a Sephadex® G-25 (Cytiva) 5 mL column. Pure *Ec*CueO preparations were subjected to a process of aliquoting, followed by freezing in liquid nitrogen, and storage at −80 °C.

2.4. UV–visible and electron paramagnetic resonance (EPR) spectroscopies

The UV–visible spectra of *Ec*CueOs were recorded using a Cary 60 UV–visible spectrophotometer (Agilent Technologies). APO enzyme preparations were diluted to 25 ± 1 μM in 40 mM MOPS buffer at pH 7.0. Subsequently, 4 equivalents of $CuSO_4$ (100 ± 1 μM) were added to the APO enzyme solution, marking the start of the incubation period. The UV–visible spectra were recorded at 5-min intervals for a total duration of 120 min. Following this period, the excess of unbound Cu^{2+} was removed using a NAP5 desalting column, previously equilibrated with 40 mM MOPS buffer at pH 7.0. Raw spectra were normalized by their absorption at 280 nm to facilitate comparison of the spectra and compensate for the dilution induced by the copper addition and protein loss after buffer exchange.

X-band CW EPR was performed on frozen solutions in EPR quartz tubes. Spectra were measured at 120 K on a Bruker EleXsys E500 spectrometer equipped with an SHQ rectangular cavity and N_2-temperature controller. For all spectra, the microwave power was set to 10 mW and the modulation amplitude to 1.6 mT. The EPR spectra of *Ec*CueO preparations were acquired for the APO enzymes and after each $CuSO_4$ addition. The Cu(II) quantification was estimated by double integration of the EPR signal using Cu-EDTA as a standard. EPR spectra were simulated using the EasySpin package (version 6.0.6) under Matlab (The MathWorks, Inc., US) [33].

2.5. Oxidative activities in solution

2,2′-azino-bis(3-ethylbenzothiazoline-6-sulfonic acid) (ABTS) was used as an electron donor for measuring the activity in solution of APO *Ec*CueOs. Enzymatic assays were conducted under air at 30 °C by monitoring the absorbance increase at 420 nm ($\varepsilon_{420\ nm}$ = 36,000 M^{-1} cm^{-1}) using a spectrophotometer microplate reader (Spark 10 M, Tecan, Switzerland). The reaction buffer was composed of 100 mM NaAcetate at a pH 5.0, with increasing concentrations of ABTS ranging from 0 to 60 mM for Michaelis-Menten quantifications, as illustrated in **Fig. S9**, and with 17 mM ABTS for assays depicted in Fig. 4. $CuSO_4$, ranging from 1 to 1000 μM, used as a source of copper for enzyme metalation, and ABTS were present into the reaction mixture prior to injection of APO enzyme, accompanied by the automated recording of enzyme kinetic data. ABTS kinetic parameters of CueOs were calculated by OriginPro 2016 (OriginLab Corporation, Massachusetts, USA), using the steady-state linear phase to make a linear fit and estimate the reaction rate. The resulting reaction rates were fitted with Michaelis-Menten equation with one site saturation:

$$V_i = \frac{V_{max} \bullet [S]}{K_m + [S]}$$

where V_i = initial speed, V_{max} = maximal initial speed, K_m = Michaelis constant and [S] = ABTS concentration.

Air-stable substrate $[Cu^{I}(BCA)_2]^{3-}$ was used for measuring the cuprous oxidase activity of the APO *Ec*CueOs as previously reported [21,24]. Briefly, 800 μM $[Cu^{I}(BCA)_2]^{3-}$ stock solution was prepared by dissolving $[Cu^{I}(CH_3CN)_4]PF_6$ in 50 mM BisTris buffer, 1.6 mM bicinchoninic acid disodium salt hydrate (BCA) at a pH 7.0 under anaerobic conditions. $[Cu^{I}(BCA)_2]^{3-}$ concentration was checked prior to measuring APO *Ec*CueO activity (ε_{562} = 7900 M^{-1} cm^{-1}). The reaction buffer was composed of 50 mM BisTris buffer at a pH 7.0 with increasing concentrations of $[Cu^{I}(BCA)_2]^{3-}$ from 0 to 400 μM for Michaelis-Menten quantifications (Fig. 5 BC), and with 50 μM $[Cu^{I}(BCA)_2]^{3-}$ for assays depicted Fig. 5 E, with the addition of free BCA^{2-} equivalent from 0.05 to 2. $[Cu^{I}(BCA)_2]^{3-}$ kinetic parameters of CueOs were calculated by OriginPro 2016 (OriginLab Corporation, Massachusetts, USA), using the first 200 s to make a linear fit and estimate the reaction rate. The resulting reaction rates were fitted with a Michaelis-Menten equation with one site saturation as above.

2.6. Preparation of the CueO-functionalized CNT based working electrodes

CueO bioelectrodes were prepared as previously reported [24]. Amino-functionalized (NH_2-CNT) CNTs generating positively charged electrode surface were used for the immobilization of the CueO. Films of CNT were made by drop casting 15 μL of CNT suspension at 1 mg mL^{-1} on a glassy carbon electrode. A 10 μL aliquot of 15 μM CueO preparation in 40 mM MOPS buffer at pH 7.0 was drop casted on the CNT-based electrode, and incubated under air for 60 min at 4 °C. The enzyme-modified electrode was washed with 40 mM MOPS buffer at pH 7.0 to remove poorly adsorbed enzymes.

2.7. Electrochemical measurements

Cyclic voltammetry (CV) and chronoamperometry (CA) experiments were carried out in a three-electrode electrochemical cell using an Autolab PGSTAT30 potentiostat, controlled by Nova software, and a rotating electrode instrument (Metrohm Autolab, Switzerland). The rotation speed (ω) of the working electrode was set to 3000 rpm. The CNT-based bioelectrodes were used as working electrodes. Pt wire was used as counter electrode and the $Hg|Hg_2SO_4|sat$, K_2SO_4 (MSE reference electrode) served as reference electrode. Potentials are referred to the Normal Hydrogen Electrode according to $E_{NHE} = E_{MSE} + 0.64$ V. All current densities are normalized with respect to the geometrical surface of the glassy carbon electrode (0.071 cm^2). The experiments were conducted at 30 °C under controlled oxygen (O_2) or nitrogen (N_2) saturated atmosphere, by continuously bubbling either O_2 or N_2 gas in the electrolyte solution. The supporting electrolyte was 100 mM NaAcetate buffer at pH 5.0 for all experiments. Additions of $CuSO_4$ to the electrolyte solution were performed at the highest potential (0.74 V *vs.* NHE) used for CV experiments. For each *Ec*CueO preparation, at least six bioelectrodes were evaluated for each electrochemical measurement.

3. Results and discussion

3.1. Structural analysis of Cu8 ligands in MCOs

We examined H_{145} conservation among a variety of MCO enzymes as a first step to validate its key physiological function (**Table S3**). It is interesting to note that, in *Ec*CueO, H_{145} belongs to a histidine motif ($H_{141}xH_{143}xH_{145}$) in which H_{141} and H_{143} participate in the coordination of one Cu-T3 (Fig. 2). The protein sequences of different MCOs have been aligned using *Ec*CueO as the reference sequence/structure for the purpose of identifying the conserved Cu8-ligands. The HxHxH motif has been identified as a conserved structural element in gram-negative metalloxidases, including CueOs, McoA, McoP and McoC (Fig. 2, **Fig. S2**).

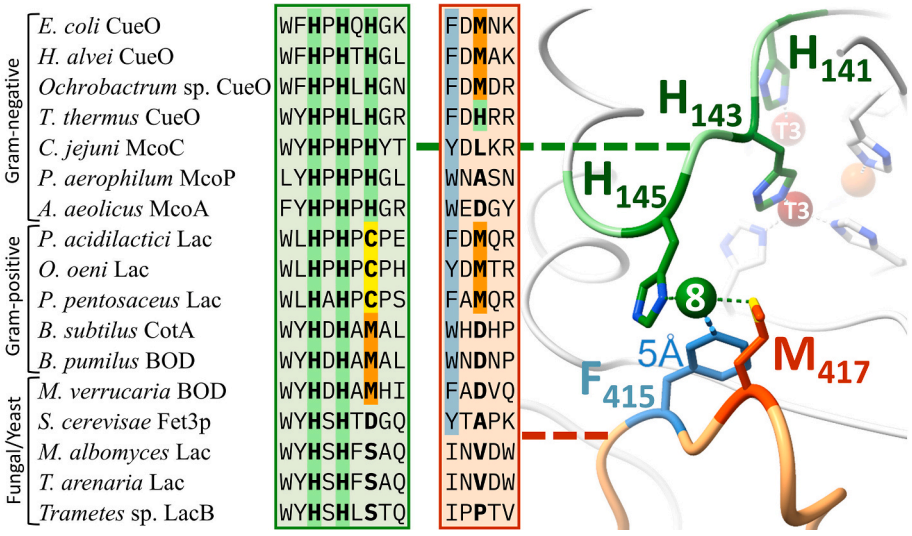

Fig. 2. Partial sequences alignment of MCO enzymes listed in Table S3. Cu8 and coordinating ligand in *E. coli* CueO is shown as a reference structure. The green box shows the histidine motif in which the first two participate in the Cu-T3 coordination, highlighted in green and bold. The orange box shows the equivalents residue of F_{415} and M_{417} in *E. coli* CueO. (For interpretation of the references to colour in this figure legend, the reader is referred to the web version of this article.)

In gram-positive laccases from lactic acid bacteria (LAB), the Cu8 histidine ligand corresponding to H_{145} in *Ec*CueO is substituted by a cysteine residue yielding the HxHxC motif (Fig. 2). It has been observed that the cysteine residue of the HxHxC motif found can be solvent accessible (*P. acidilactici*) or involved in a disulfide bond with a close cysteine residue from an adjacent loop (*P. pentosaceus*) or a C-terminal His/Met-rich tail (*O. oeni*) (**Fig. S3**) [36,37]. Moreover, the partially or fully-solved C-terminal His/Met-rich tail is oriented toward or surrounds the Cu8-site and coordinating ligands (**Fig. S3**) [36,37]. Recent structural findings obtained on *P. pentosaceus* laccase demonstrate that the Cu8-site and its coordination are conserved in LAB laccases [38]. The Cu8 coordination involves the carbonyl oxygen of the cysteine from the HxHxC motif, the methionine equivalent to M_{417} in *Ec*CueO, and the additional contribution of two methionine residues from the C-terminal His/Met-rich tail (**Fig. S3**) [38]. In gram-positive enzymes, such as *B. pumilus* BOD and *B. subtilus* CotA, the Cu8 histidine ligand is exchanged for methionine, yielding a HxHxM motif (Fig. 2, **Fig. S4**). An additional disordered loop rich in histidine residues (His-rich) covers the Cu8-site (**Fig. S4**). It is probable that the histidine exchange to methionine in the HxHxM motif in these enzymes is compensated by one proximal histidine residue from the His-rich loop (**Fig. S5A**). The HxHxM motif loop observed in the bacterial BOD is also observed in fungal BOD (*M. verrucaria*) with no surrounding His-rich loop, however (**Fig. S5B**), indicating that the function of this additional flexible domain can be bypassed. In fungal laccases a non-coordinating serine replaces the Cu8-ligand (Fig. 2**, Fig. S6**).

In summary, this structural analysis of Cu8-site coordination in MCOs, highlights the broad conservation of the HxHx(H/C/M) motif, suggesting H_{145} in CueOs should have a pivotal role. Based on our previous studies, we hypothesized this function should be link to metalation in the presence of copper [32].

3.2. Expression and isolation of copper-free (APO) EcCueOs

To assess this function, both *Ec*CueO WT and the H_{145}S variant were studied starting from copper-free (APO) enzymes and evaluating the impact of the addition of exogeneous copper. Within this objective, *Ec*CueOs were cultivated in a medium devoid of exogenous copper, and the protein purification process was conducted for both *Ec*CueO WT and H_{145}S, omitting the *in vitro* copper insertion step. Consequently, this led to the isolation of APO CueOs. The APO *Ec*CueOs were found to be colorless, and minimal traces of copper were detected by ICP-OES in the range of 0.2–0.3 Cu per CueO enzyme (**Table S4**). These traces likely arose from the expression medium.

3.3. Spectroscopic characterization of EcCueO metalation

The metalation of APO *Ec*CueO WT and H_{145}S in the presence of Cu^{2+} ions was then investigated using UV–visible and EPR spectroscopies. These methodologies enable the selective identification of CueO cofactors, Cu-T1 and Cu-T3 with UV–visible spectroscopy and Cu-T1 and Cu-T2 with EPR spectroscopy. As expected, the APO *Ec*CueOs lack the absorption signals characteristic of MCOs, *i.e.* the peak at 610 nm, attributed to ligand-to-metal charge transfer between the cysteine thiolate and Cu-T1, and the shoulder around 330 nm indicative of the presence of Cu-T3 (Fig. 3A**,** dashed lines). The addition of 4 equivalents $CuSO_4$ instantaneously turned both WT and variant protein solutions from colorless to blue, with concomitant occurrence of the 610 nm peak, indicating a rapid coordination of Cu-T1 (**Fig. S7**). Absorbance at 330 nm was monitored over time (Fig. 3B**, Fig. S7**). For the WT enzyme, the maximum of absorbance at 330 nm was achieved after approximately 30–40 min. In the case of the H_{145}S variant, however, this process required 2–3 times longer, indicating a slower metalation rate of the Cu-T3 site. Following a period of incubation lasting 2 h, the excess of unincorporated Cu^{2+} was removed by passing the enzymatic preparations through a desalting column. Copper content was quantified by ICP-OES revealing a value close to 4, as expected for MCOs (**Table S4**). After this 2-h incubation time, the absorbance at 610 nm and 330 nm of both Cu-incorporated CueOs are shown comparable (Fig. 3A**,** full lines).

The EPR spectra of both APO *Ec*CueOs exhibited a weak g-perpendicular signal, consistent with copper traces measured by ICP-OES (Fig. 3C**, Table S4**). The amount of copper is too low however to detect g-parallel signals, which is consistent with the colorless solutions and UV–visible spectra. The incorporation of copper into the Cu-T1 and Cu-T2 sites of the APO *Ec*CueOs was monitored by adding subsequent equivalents of $CuSO_4$ from 0.1 to 2 (Fig. 3C). Following each addition of Cu^{2+}, the *Ec*CueO enzymatic preparations were rapidly frozen in liquid nitrogen, with a total incubation period of 16 min prior to measurement. Double integration of the EPR signals enables the quantification of the Cu^{2+} content (**Table S5**). Up to 2 equivalents of $CuSO_4$, the EPR signals account for approximately 2 equivalents of paramagnetic copper, with the EPR spectra of the H_{145}S variant demonstrating a high degree of similarity to those of the WT *Ec*CueO. This finding confirms that the absence of H_{145} does not affect the metalation of the Cu-T1, as shown

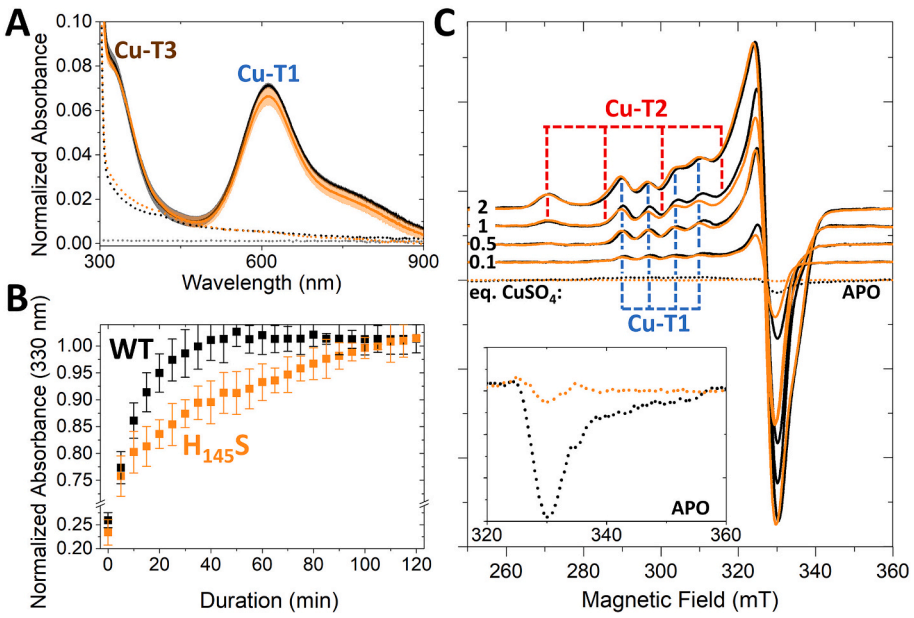

Fig. 3. (A) Normalized UV–visible absorption spectra of *Ec*CueOs: WT APO (black, dashed line), $H_{145}S$ APO (orange, dashed line), WT Cu-incorporated (black, full line with pale shadow corresponding to standard deviation) and $H_{145}S$ Cu-incorporated (orange, full line with pale shadow corresponding to standard deviation). 40 mM MOPS buffer at pH 7.0 serves as the baseline (light gray dashed). The spectra are normalized to their respective absorption at 280 nm. (B) Normalized absorption at 330 nm of *Ec*CueOs overtime in presence of 4 equivalents of $CuSO_4$. Values are normalized between 0 and 1 respectively for the baseline (40 mM MOPS buffer at pH 7.0) and the relative maximum of absorbance reached by each *Ec*CueO after the addition of $CuSO_4$. (C) EPR spectra of APO *Ec*CueOs WT (black dashed) and $H_{145}S$ (orange dashed) and in presence of increasing equivalents of $CuSO_4$: 0.1, 0.5, 1 and 2 (full lines). Spectra are offset along the y-axis for clarity. Inset: zoom on the g perpendicular signals of APO *Ec*CueOs. Experimental conditions: 40 mM MOPS buffer at pH 7.0, temperature = 120 K, microwave power = 10 mW at 9413 MHz; modulation amplitude, 1.6 mT at 100 kHz.

above by UV–visible analysis. Moreover, the EPR data indicate that H_{145} does not influence Cu-T2 site completion either, as demonstrated by the spectral simulations (**Fig. S8 and Table S6**).

3.4. *Implication of H_{145} in CueO metalation and catalysis in presence of Cu^{2+}*

The spectroscopic data presented herein suggest that although the absence of H_{145} does not alter the composition of the Cu-T1, Cu-T2, and Cu-T3 cofactors within the MCO, its absence does influence the kinetics of cofactor assembly. Specifically, the $H_{145}S$ variant exhibited a delayed temporal progression of Cu-T3 absorption in comparison to the WT enzyme suggesting a potential involvement of H_{145} in the TNC maturation of APO *Ec*CueO in the presence of Cu^{2+}. To ascertain this role, activity tests were conducted using ABTS. ABTS is a model substrate that is frequently utilized in the study of the oxidase activity of MCOs. The ABTS oxidation requires the presence of the fully metalated Cu-T1 and TNC, *i.e.* HOLO CueO. ABTS activity tests, therefore serve as an indirect measurement of metalation progress (**Fig. S9** and **Table S7**). The increase in the absorption at 420 nm indicative of the catalytical oxidation of ABTS was monitored *in situ* upon increasing Cu^{2+} concentrations (Fig. 4). The APO *Ec*CueOs WT, $H_{145}S$ variant as well as ΔCu5 variant, in which two of the four coordinating residues were mutated ($D_{439}A$, $M_{441}Q$), leading to its inability to coordinate Cu^{2+} at the Cu5 site [24], were tested (**Fig. S9**). Each kinetic curve displayed a distinct initial lag phase, that preceded the steady-state catalysis. This lag phase was absent in our previous study using HOLO *Ec*CueO, strongly suggesting that it is due to the time required for enzyme metalation [24]. The initial lag phase of the ΔCu5 enzyme is similar to that of the WT enzyme (Fig. 4), further supporting the conclusion that the Cu5 site, required for CueO-like enzymes to enhance ABTS oxidation, is not involved in the process [18,21,24,39,40]. Across all tested concentrations of $CuSO_4$, the $H_{145}S$ variant invariably exhibited a prolonged activation delay compared to the WT, with the delay being more pronounced at the lowest Cu^{2+} concentrations.

These results provide compelling evidence that exogeneous Cu^{2+} can induce the metalation of *Ec*CueOs, thereby allowing for catalytical ABTS oxidation. The prolonged lag phase exhibited by the *Ec*CueO $H_{145}S$ variant is therefore specifically associated with the absence of the H_{145}, aligning with the delayed temporal progression of Cu-T3 formation as demonstrated by UV–visible spectroscopy. Collectively, these findings suggest that the absence of H_{145} significantly impairs *Ec*CueO metalation in the presence of Cu^{2+}, a phenomenon particularly pronounced at sub-micromolar $CuSO_4$ concentrations.

3.5. *Implication of H_{145} in CueO metalation and catalysis in presence of Cu^{+}*

The primary catalytic function of CueOs is the oxidation of cuprous ions to the less toxic cupric state. In the physiological context, APO *Ec*CueO undergoes periplasmic translocation in response to copper stress [41]. The metalation of the APO *Ec*CueO could represent an initial copper detoxification function [41], whereby four copper atoms are acquired (Cu-T1 and TNC) and subsequently utilized for cuprous oxidation. Under stress conditions, both Cu^{+} and Cu^{2+} can be found in the periplasmic environment. We thus aimed to investigate whether and how functional metalation of APO *Ec*CueOs can occur in the presence of Cu^{+} instead of Cu^{2+}. The $[Cu^{I}(BCA)_2]^{3-}$ complex is often employed for the delivery of Cu^{+} to cuproproteins and the indirect measurement of the Cu^{+} affinity [24,42–46]. In the present study, we used this complex as a source of Cu^{+} to metalate the APO *Ec*CueOs, and subsequently to assess the cuprous oxidase activity of the enzymatic preparations in solution.

A notable distinction was observed when comparing this approach to ABTS oxidation in the presence of unchelated Cu^{2+}. Indeed, the initial lag phase was completely abolished for both *Ec*CueO WT and the $H_{145}S$ variant (Fig. 5A). This finding indicates that the rate of metalation in the presence of chelated Cu^{+} is faster than the experimental timescale,

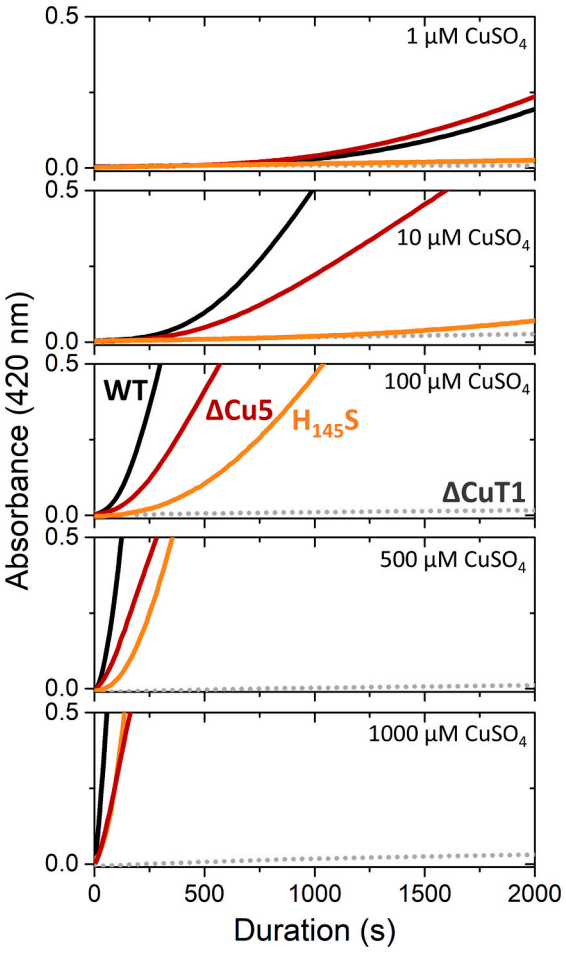

Fig. 4. ABTS oxidation activity of APO *Ec*CueOs: WT (black), ΔCu5 (red), $H_{145}S$ (orange) and inactive ΔCu-T1 as a control (gray dashed). Assays performed in 100 mM NaAcetate buffer at pH 5.0, 17 mM ABTS, 0.1 µM of APO-CueO and different $CuSO_4$ concentrations: 1 µM, 10 µM, 100 µM, 500 µM and 1000 µM. The initial ABTS absorption was subtracted from the kinetics in order to start from 0. (For interpretation of the references to colour in this figure legend, the reader is referred to the web version of this article.)

irrespective of the presence of H_{145}. Subsequently, the linear steady-state catalysis is followed by progressive inhibition caused by the excess of free BCA produced during the catalytic oxidation of the complex. This phenomenon has been previously described by Djoko et al. [47].

The oxidation rate of $[Cu^{I}(BCA)_2]^{3-}$ was measured at several complex concentrations, resulting in apparent Michaelis-Menten behavior (Fig. 5BC, **Table S8**). The apparent catalytic efficiency ($V_{max}/_{app}K_m$) is comparable among WT and $H_{145}S$ variant, suggesting that cuprous oxidation of *in situ* metalated HOLO enzymes is not affected by the absence of H_{145}. Given the rapid reaction of *Ec*CueOs with $[Cu^{I}(BCA)_2]^{3-}$ under the experimental time constraints employed, a strategy was developed to decelerate the metalation process and potentially differentiate between the WT and $H_{145}S$ variant. This strategy entailed increasing the BCA^{2-} concentration, thereby enhancing Cu^{+} complexation and diminishing the availability of free Cu^{+} (Fig. 5D). When measuring the oxidation of $[Cu^{I}(BCA)_2]^{3-}$ in the presence of increasing concentrations of free BCA^{2-}, a lag phase progressively emerged for both APO *Ec*CueOs (Fig. 5E**)**. Notably, the $H_{145}S$ variant demonstrated a prolonged lag phase in comparison to the WT *Ec*CueO. The impact of free BCA^{2-} on the $H_{145}S$ variant activity compared to the WT protein is also clearly reflected in the reaction rate values (Fig. 5F). An exponential decay of the cuprous oxidase activity can be observed for both *Ec*CueOs, but more significantly in the case of $H_{145}S$ variant (Fig. 5F).

Thus, by adjusting the Cu^{+}:BCA ratio, the availability of free Cu^{+} is modulated (Fig. 5D), which in turn impacts the metalation rate. The lowest BCA^{2-} excess (0.05) used in the current work is enough to distinguish between the WT *Ec*CueO and the $H_{145}S$ variant. This typical ratio corresponds to a concentration of free Cu^{+} in the range of 10^{-10}–10^{-11} M (Fig. 5D). H_{145} thus appears as mandatory under conditions of sub-picomolar Cu^{+} concentration, in line with the requirement of fast APO CueO metalation to detoxify the periplasmic environment from toxic Cu^{+}.

3.6. *Electrometalation of APO EcCueOs*

In a next step, following the approach developed in [32], electrochemistry was employed to further investigate the metalation of APO *Ec*CueOs with the aim of elucidating the potential role of H_{145}. The interest in this methodology within our current investigation is that it allows precise tuning of non-chelated Cu^{+} levels by modulation of the potential applied for electroreduction of Cu^{2+} in the vicinity of the immobilized *Ec*CueOs.

For this purpose, the APO *Ec*CueOs were immobilized on NH_2-CNT-electrode, a surface known to allow efficient DET-type ORR by HOLO enzymes [21,24,30,32]. As shown in Fig. 6AB, APO *Ec*CueOs induced very weak ORR catalytic currents at the first CV cycle, which was close to zero for the $H_{145}S$ bioelectrode. Such a result was expected with non-active enzymes as APO ones. Less expectedly, the WT bioelectrode exhibited an ORR activation during consecutive CV scans, before any Cu^{2+} addition (Fig. 6A**).** Each CV cycle is characterized by an activation peak during the reverse scan, similar to the one shown in the inset of Fig. 6A, occurring at around 0.35–0.4 V *vs.* NHE. Following the completion of ten cycles, a stable current was reached. After addition of 10 µM $CuSO_4$ in the electrolyte following the first CV cycle, a boost of the ORR activation magnitude was observed, the catalytic current reaching the maximal current density in few subsequent cycles (Fig. 6C). It is noteworthy that the transfer of the WT bioelectrode to a copper-free supporting electrolyte did not modify the magnitude of the catalytic current, ensuring that the activation process is not linked to Cu^{+}-oxidase activity (Fig. 6C**, Table S8**). We propose that the ORR activation is associated with the progressive enzyme metalation following Cu^{+} electrogeneration. The source of Cu^{2+} before any exogeneous Cu^{2+} addition is questionable and will be discussed further below.

The behavior of $H_{145}S$ variant is markedly different. Actually, the absence of H_{145} severely impacts the ORR activation, as $H_{145}S$ variant did not allow any catalytic current to be observed after subsequent cycles under O_2 in the absence of exogenous Cu^{2+} addition (Fig. 6B). The ORR activation process can only be observed after the addition of 10 µM $CuSO_4$ to the electrolyte solution (Fig. 6D). One more difference between the $H_{145}S$ variant and the WT protein is that in order to induce an electrometalation process as fast as with the WT bioelectrode, the $H_{145}S$ bioelectrode requires the presence of at least 500 µM $CuSO_4$ in the supporting electrolyte against 10 µM for the WT bioelectrode (**Fig. S10**). It is then reasonable to propose that Cu^{2+} binding to H_{145} at the Cu8-site is the first step of the electrometalation process. Then the application of a potential sufficient to generate Cu^{+} accelerates the *in vitro* metalation and catalytic activation of CNT-immobilized *Ec*CueOs.

The difference in ORR activation between WT and $H_{145}S$ CueOs prior to any exogenous Cu^{2+} addition reflects the previously noted requirement of H_{145} for effective metalation under low-copper conditions. The APO enzymes contain only traces of copper (**Table S4**), whose primary source should originate from the expression medium solution. The extent of the ORR activation appears to be influenced by the amount of APO *Ec*CueO and the duration of the protein's incubation at the electrode (**Fig. S11**). These findings suggests that copper release could arise from the immobilization step, as previously concluded [32].

To support this conclusion, the APO *Ec*CueO bioelectrodes were

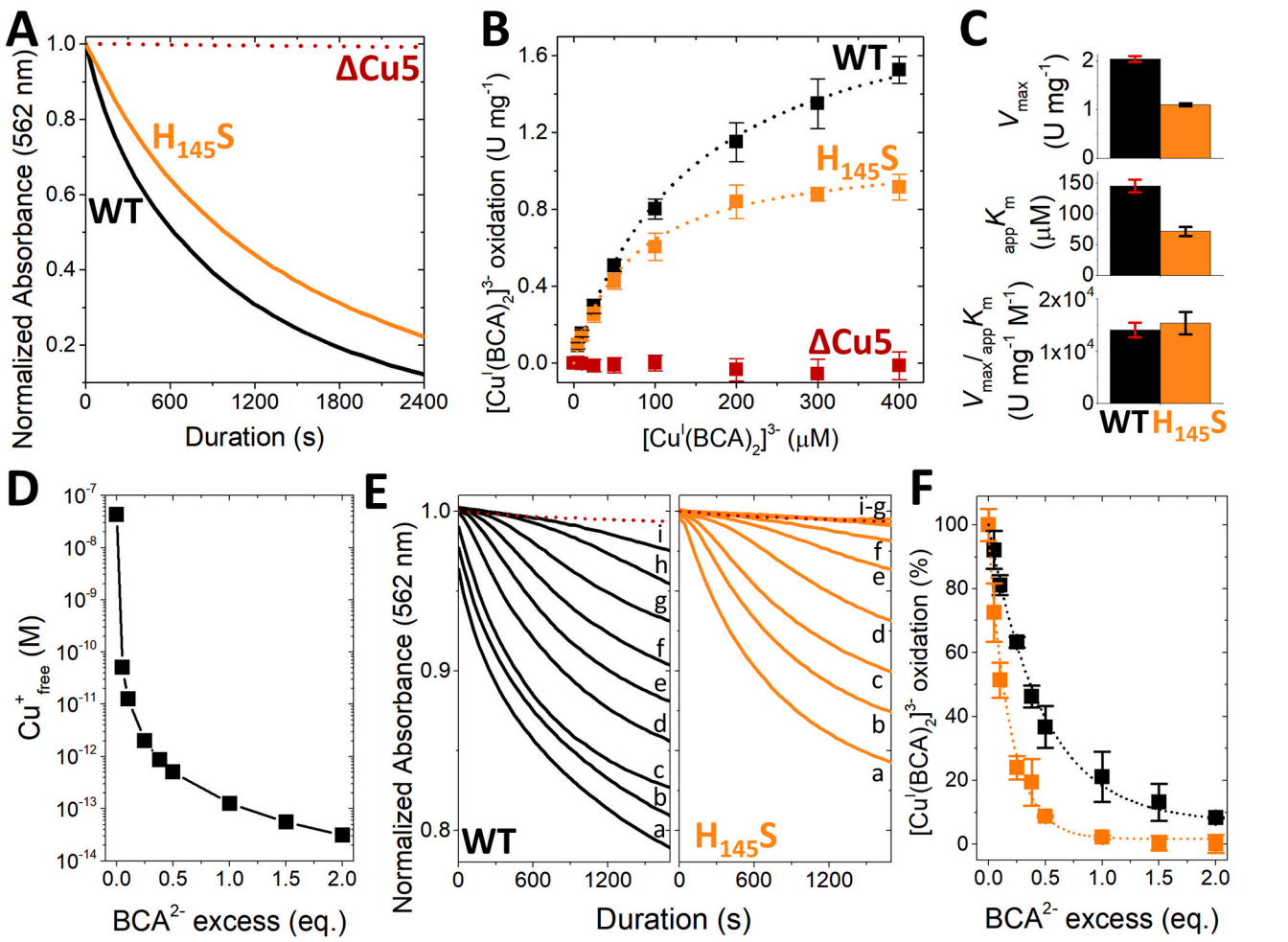

Fig. 5. (A) $[Cu^{I}(BCA)_2]^{3-}$ oxidation activity of APO *Ec*CueOs: WT (black), $H_{145}S$ (orange). The cuprous oxidase inactive ΔCu5 is given as a control (red dashed). Spectrometric assays performed in 50 mM Bis Tris buffer at pH 7.0, 50 μM $[Cu^{I}(BCA)_2]^{3-}$ (Cu^{+}:BCA^{2-} ratio of 1:2) and 0.05 μM of APO-CueO. The initial $[Cu^{I}(BCA)_2]^{3}$ absorption was normalized between 0 and 1. (B) Michaelis-Menten fits (dashed lines) for oxidation of $[Cu^{I}(BCA)_2]^{3-}$ complex (Cu^{+}:BCA^{2-} ratio of 1:2). (C) V_{max}, $_{app}K_m$, and apparent catalytic efficiency ($V_{max}/_{app}K_m$) derived from Michaelis-Menten fits. (D) Concentration of free Cu^{+} in 50 mM Bis Tris buffer at pH 7.0 solution containing 50 μM $[Cu^{I}(BCA)_2]^{3-}$ (Cu^{+}:BCA^{2-} ratio of 1:2) and an excess of BCA^{2-} from 0 to 2 equivalents. (E) $[Cu^{I}(BCA)_2]^{3-}$ oxidation activity of APO *Ec*CueOs at different Cu^{+}:BCA^{2-} ratios: WT (black), $H_{145}S$ (orange). The inactive cuprous oxidase ΔCu5 is given as a control (red dashed). Spectrometric assays performed in 50 mM Bis Tris buffer at pH 7.0, 50 μM $[Cu^{I}(BCA)_2]^{3-}$ (Cu^{+}:BCA^{2-} ratio of 1:2), 0.05 μM of APO-CueO with the addition of an excess of BCA^{2-}: 0 (a), 0.05 (b), 0.1 (c), 0.25 (d), 0.38 (e), 0.5 (f), 1 (g), 1.5 (h), 2 (i). The initial $[Cu^{I}(BCA)_2]^{3}$ absorption was normalized in order to start from 1. (F) Rate of $[Cu^{I}(BCA)_2]^{3-}$ oxidation by APO *Ec*CueOs: WT (black) and $H_{145}S$ (orange), expressed in percentage. Dashed lines represent the exponential decay fit of the activity in presence of an excess of BCA^{2-}. Experimental conditions refer to (E).

maintained at an applied potential of 0.63 V *vs.* NHE, sufficiently high to minimize the formation of electroreduced Cu^{+}. Accordingly, in the absence of exogeneous Cu^{2+} addition, no activation can be observed whatever the *Ec*CueO enzyme (Fig. 7A). However, the addition of 100 μM and subsequently 500 μM $CuSO_4$ induced an activation of the ORR for both bioelectrodes, with a much lower activation observed for the $H_{145}S$ *Ec*CueO (Fig. 7A). Such a result may signify that H_{145} is required for Cu^{2+} binding at Cu8 and subsequent activation process. However, 100 μM or 500 μM $CuSO_4$ addition results in the electrogeneration of Cu^{+} in the subpicomolar range at the applied potential of 0.63 V (Fig. 7B). These concentrations align with those calculated in the presence of an excess of BCA^{2-}, suggesting that CueO electroassisted metalation occurs with these very low electrogenerated Cu^{+} concentrations. The absence of H_{145} residue slows down the *in situ* electrometalation process.

4. Conclusion

This study has advanced our understanding of the metalation mechanism of multicopper oxidases, which are key enzymes in numerous biological and biotechnological processes. Using spectroscopic assays with Cu^{2+} or Cu^{+} and electrochemistry, we demonstrated that H_{145} plays a pivotal role in the maturation and metalation of *Ec*CueO, under conditions of limited copper availability within the protein environment. We proposed that Cu^{2+} binding at the Cu8-site initiated CueO metalation by Cu^{+}. In agreement with this hypothesis, we recently reported the affinity constant of the Cu^{2+}-binding site of pseudopeptides [48]. An enhanced affinity when a histidine ligand is present at the place of a methionine or a serine residue was measured. We also demonstrated that the fast cofactor insertion into APO *Ec*CueO can occur under subpicomolar Cu^{+} concentrations. The absence of ORR inactivation using HOLO $H_{145}S$ bioelectrodes [31] would be indirect evidence that the function of the Cu8-site in enzyme metalation is affected compared to the WT enzyme.

The *in-silico* analysis highlights a conserved HxHx(H/C/M) motif among various prokaryotic MCOs. This observation suggests the presence of a common Cu8 primary ligand for the metalation under physiological conditions. Based on the current work, the absence of Cu8-site

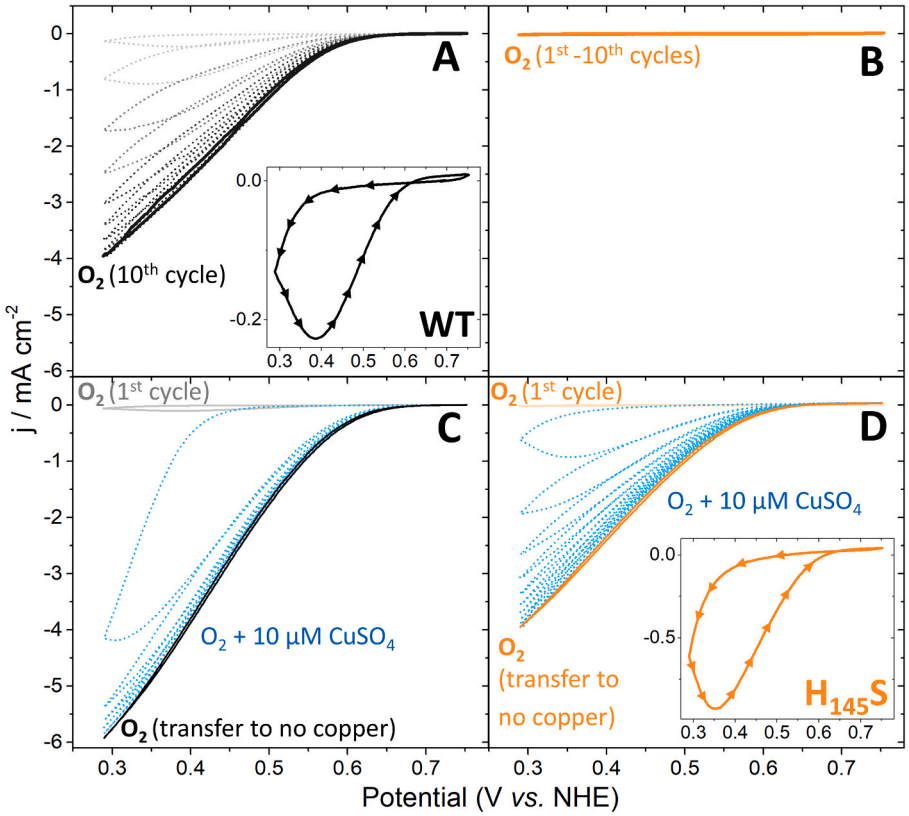

Fig. 6. Electrochemical activity of APO *Ec*CueO-functionalized NH_2-CNT electrode. CVs under O_2 after 60 min of protein (10 µL at 15 µM) immobilization for (A) WT and (B) $H_{145}S$ variant. The inset in (A) is a zoom of the first cycle of the WT bioelectrode. CVs under O_2 and in the presence of 10 µM $CuSO_4$ (blue lines) for (C) WT and (D) $H_{145}S$ variant. The inset in (D) is a zoom of the first cycle of the $H_{145}S$ bioelectrode. The CVs labelled "O_2 (transfer to no copper)" represent the bioelectrodes response after transfer to a copper-free supporting electrolyte. Experimental conditions: 100 mM NaAcetate buffer, pH 5.0 at 30 °C, ω = 3000 rpm, v = 5 mV s^{-1}. (For interpretation of the references to colour in this figure legend, the reader is referred to the web version of this article.)

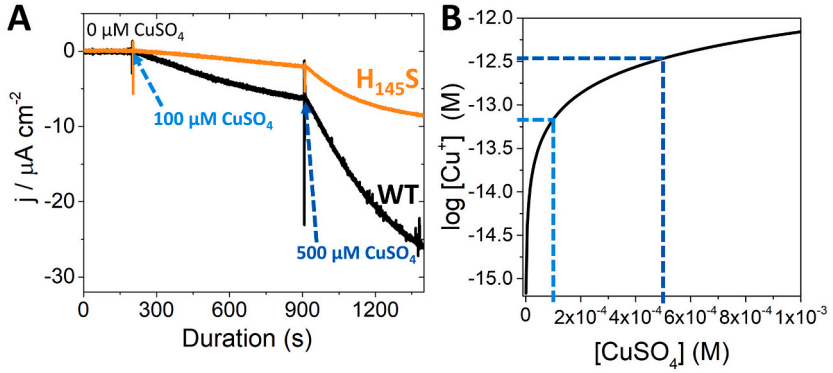

Fig. 7. A) Electrochemical activity of APO *Ec*CueO-functionalized NH_2-CNT electrodes. CA at 0.63 V *vs.* NHE under O_2 (0–200 s) and in presence of 100 µM $CuSO_4$ (200–900 s) and 500 µM $CuSO_4$ (900–1400 s). Experimental conditions: 100 mM NaAcetate buffer, pH 5.0 at 30 °C, ω = 3000 rpm. B) Equilibrium concentration of Cu^+ at the applied potential 0.63 V *vs.* NHE as a function of the amount of added $CuSO_4$ in 100 mM NaAcetate buffer, pH 5.0 at 30 °C. The dashed lines indicate the amount of Cu^+ electroreduced in presence of 100 µM $CuSO_4$ (cyan) and 500 µM $CuSO_4$ (blue). (For interpretation of the references to colour in this figure legend, the reader is referred to the web version of this article.)

in certain MCOs may indirectly indicate that these enzymes are metalated in an environment with sufficiently copper availability (Fig. 2). Accordingly, eukaryotic APO-MCOs are metalated in subcellular compartment enriched with Cu^+ [49–53]. In the physiological context, copper is mostly reduced to the cuprous state and bound to metallochaperones or molecules (*i.e.* glutathione) [54–58]. It can be hypothesized that the Cu8-site may play a role in the maturation of APO MCOs *in vivo*, serving as a transient recognition site for Cu-chaperones/molecules, facilitating cofactor insertion into the APO MCOs. The presence of a His/Met-rich or a His-rich insertions surrounding the Cu8-site in bacterial MCOs suggests the potential for the functional modulation of the Cu8-site. A function analogous to that demonstrated for CueO His/Met-rich domain in Cu^+ recruitment can be postulated for this additional insertion [21,24]. Indeed, in the case of LAB laccases, the Cu8 proximal His/Met-rich insertion contributes to its coordination by providing two additional methionine ligands [38]. The latter study lends support to the hypothesis that these MCO subfamilies are expressed within a physiological environment characterized by low Cu

availability. The hypothesis that the flexibility of His/Met-rich insertions plays a pivotal role in the recruitment of the copper cofactor remains to be substantiated through further investigation.

Beyond these fundamental advances in our understanding of crucial enzymes such as multicopper oxidases, our findings might have significant applications in medicine and environmental biotechnology. The functional metalation of MCOs through Cu8-site can facilitate comprehension of the mechanisms of copper trafficking and acquisition by MCO enzymes involved in copper and iron homeostasis. A particularly relevant case study, is that of human ceruloplasmin, a 6dMCO that has been implicated in neurodegenerative diseases [59–61]. The capacity of the APO *Ec*CueO WT to scavenge traces of Cu^{+}/Cu^{2+} demonstrated in the present study, can also be exploited for the development of electrochemical biosensors for the sensitive detection of copper in the environment.

CRediT authorship contribution statement

Paolo Santucci: Investigation, Formal analysis. **Frédéric Biaso:** Investigation, Formal analysis. **Jérôme Becam:** Investigation, Formal analysis. **Ludovic Dubard:** Investigation, Formal analysis. **Marianne Ilbert:** Writing – review & editing, Formal analysis. **Benjamin Ezraty:** Writing – review & editing, Validation. **Ievgen Mazurenko:** Writing – review & editing, Writing – original draft, Investigation. **Elisabeth Lojou:** Writing – review & editing, Writing – original draft, Funding acquisition. **Umberto Contaldo:** Writing – review & editing, Writing – original draft, Supervision, Investigation, Formal analysis, Conceptualization.

Declaration of competing interest

The authors declare no competing financial interest.

Acknowledgements

This work was supported by the National Research Agency (ANR, France) under the grant MetCop (ANR-21-CE44-0024). This work also received support from the French government under the France 2030 investment plan, as part of the Initiative d'Excellence d'Aix-Marseille Université—A*MIDEX (AMX-21-PEP-001). We are grateful to the EPR-MRS facilities of Aix-Marseille University EPR center and the French research infrastructure INFRANALYTICS (FR2054).

Appendix A. Supplementary data

Supplementary data to this article can be found online at https://doi.org/10.1016/j.jinorgbio.2026.113257.

References

[1] P.J. Hoegger, S. Kilaru, T.Y. James, J.R. Thacker, U. Kües, Phylogenetic comparison and classification of laccase and related multicopper oxidase protein sequences, FEBS J. 273 (2006) 2308–2326.
[2] D. Sirim, F. Wagner, L. Wang, R.D. Schmid, J. Pleiss, The laccase engineering database: a classification and analysis system for laccases and related multicopper oxidases, Database 2011 (2011) 1–7.
[3] I. Mazurenko, T. Adachi, B. Ezraty, M. Ilbert, K. Sowa, E. Lojou, Electrochemistry of copper efflux oxidase-like multicopper oxidases involved in copper homeostasis, Curr. Opin. Electrochem. 32 (2022) 100919.
[4] G. Molpeceres, P. Aza, I. Ayuso-Fernández, G. Padilla, F.J. Ruiz-Dueñas, S. Camarero, Deciphering the distribution and types of multicopper oxidases in Basidiomycota fungi, Mol. Phylogenet. Evol. 206 (2025).
[5] M. Lang, M.R. Kanost, M.J. Gorman, Multicopper Oxidase-3 is a laccase associated with the peritrophic matrix of Anopheles gambiae, PLoS One 7 (2012) e33985, https://doi.org/10.1371/journal.pone.0033985.
[6] Q. Li, X. Wang, M. Korzhev, H.C. Schröder, T. Link, M.N. Tahir, B. Diehl-Seifert, W. E.G. Müller, Potential biological role of laccase from the sponge Suberites domuncula as an antibacterial defense component, Biochim. Biophys. Acta 1850 (2015) 118–128.
[7] M. Chen, J. Zheng, G. Liu, E. Xu, J. Wang, B.K. Fuqua, C.D. Vulpe, G.J. Anderson, H. Chen, Ceruloplasmin and hephaestin jointly protect the exocrine pancreas against oxidative damage by facilitating iron efflux, Redox Biol. 17 (2018) 432–439.
[8] E.I. Solomon, R.K. Szilagyi, S. DeBeer George, L. Basumallick, Electronic structures of metal sites in proteins and models: contributions to function in blue copper proteins, Chem. Rev. 104 (2004) 419–458, https://doi.org/10.1021/cr0206317.
[9] E.I. Solomon, U.M. Sundaram, T.E. Machonkin, Multicopper oxidases and oxygenases, Chem. Rev. 96 (1996) 2563–2606, https://doi.org/10.1021/cr950046o.
[10] M. Valles, A.F. Kamaruddin, L.S. Wong, C.F. Blanford, Inhibition in multicopper oxidases: a critical review, Catal. Sci. Technol. 10 (2020) 5386–5410, https://doi.org/10.1039/D0CY00724B.
[11] S. Callejón, R. Sendra, S. Ferrer, I. Pardo, Cloning and characterization of a new laccase from Lactobacillus plantarum J16 CECT 8944 catalyzing biogenic amines degradation, Appl. Microbiol. Biotechnol. 100 (2015) 3113–3124.
[12] S. Callejón, R. Sendra, S. Ferrer, I. Pardo, Recombinant laccase from *Pediococcus acidilactici* CECT 5930 with ability to degrade tyramine, PLoS One (2017) 1–19.
[13] S. Wongwattanarat, A. Schorn, L. Klose, C. Carré, A.M. Romero, A. Liese, P. Pérez-garcía, W.R. Streit, A combined chemo-enzymatic treatment for the oxidation of epoxy-based carbon fiber-reinforced polymers (CFRPs), Front. Bioeng. Biotechnol. (2025) 1–15, https://doi.org/10.3389/fbioe.2025.1670548.
[14] H. Wang, X. Liu, J. Zhao, Q. Yue, Y. Yan, Z. Gao, Y. Dong, Z. Zhang, Y. Fan, J. Tian, N. Wu, Y. Gong, Crystal structures of multicopper oxidase CueO G304K mutant: structural basis of the increased laccase activity, Sci. Rep. 8 (2018) 1–12.
[15] M. Akter, C. Inoue, H. Komori, N. Matsuda, T. Sakurai, K. Kataoka, Y. Higuchi, N. Shibata, Biochemical, spectroscopic and X-ray structural analysis of deuterated multicopper oxidase CueO prepared from a new expression construct for neutron crystallography, Acta Crystallogr. Sect. F 72 (2016) 788–794, https://doi.org/10.1107/S2053230X1601400X.
[16] S.A. Roberts, G.F. Wildner, G. Grass, A. Weichsel, A. Ambrus, C. Rensing, W. R. Montfort, A labile regulatory copper ion lies near the T1 copper site in the multicopper oxidase CueO, J. Biol. Chem. 278 (2003) 31958–31963.
[17] B. Sana, S.M.Q. Chee, J. Wongsantichon, S. Raghavan, R.C. Robinson, F. J. Ghadessy, Development and structural characterization of an engineered multi-copper oxidase reporter of protein-protein interactions, J. Biol. Chem. 294 (2019) 7002–7012, https://doi.org/10.1074/jbc.RA118.007141.
[18] K. Kataoka, H. Komori, Y. Ueki, Y. Konno, Y. Kamitaka, S. Kurose, S. Tsujimura, Y. Higuchi, K. Kano, D. Seo, T. Sakurai, Structure and function of the engineered multicopper oxidase CueO from Escherichia coli-deletion of the methionine-rich helical region covering the substrate-binding site, J. Mol. Biol. 373 (2007) 141–152.
[19] H. Komori, R. Sugiyama, K. Kataoka, Y. Higuchi, T. Sakurai, An O-Centered structure of the trinuclear copper center in the Cys500Ser/Glu506Gln mutant of CueO and structural changes in low to high X-ray dose conditions, Angew. Chem. Int. Ed. 51 (2012) 1861–1864, https://doi.org/10.1002/anie.201107739.
[20] S.A. Roberts, A. Weichsel, G. Grass, K. Thakali, J.T. Hazzard, G. Tollin, C. Rensing, W.R. Montfort, Crystal structure and electron transfer kinetics of CueO, a multicopper oxidase required for copper homeostasis in Escherichia coli, Proc. Natl. Acad. Sci. 99 (2002) 2766–2771, https://doi.org/10.1073/pnas.052710499.
[21] U. Contaldo, P. Santucci, A. Vergnes, P. Leone, J. Becam, F. Biaso, M. Ilbert, B. Ezraty, E. Lojou, I. Mazurenko, How the larger methionine-rich domain of CueO from hafnia alvei enhances cuprous oxidation, JACS Au 5 (2025) 1833–1844.
[22] R.S. Granja-Travez, R.C. Wilkinson, G.F. Persinoti, F.M. Squina, V. Fülöp, T.D. H. Bugg, Structural and functional characterisation of multi-copper oxidase CueO from lignin-degrading bacterium Ochrobactrum sp. reveal its activity towards lignin model compounds and lignosulfonate, FEBS J. 285 (2018) 1684–1700.
[23] S.K. Singh, S.A. Roberts, S.F. McDevitt, A. Weichsel, G.F. Wildner, G.B. Grass, C. Rensing, W.R. Montfort, Crystal structures of multicopper oxidase CueO bound to copper(I) and silver(I): functional role of a methionine-rich sequence, J. Biol. Chem. 286 (2011) 37849–37857.
[24] U. Contaldo, D. Savant-Aira, A. Vergnes, J. Becam, F. Biaso, M. Ilbert, L. Aussel, B. Ezraty, E. Lojou, I. Mazurenko, Methionine-rich domains emerge as facilitators of copper recruitment in detoxification systems, Proc. Natl. Acad. Sci. 121 (2024) e2402862121, https://doi.org/10.1073/pnas.2402862121.
[25] C. Rensing, G. Grass, Escherichia coli mechanisms of copper homeostasis in a changing environment, FEMS Microbiol. Rev. 27 (2003) 197–213.
[26] S.K. Singh, G. Grass, C. Rensing, W.R. Montfort, Cuprous oxidase activity of CueO from Escherichia coli, J. Bacteriol. 186 (2004) 7815–7817.
[27] J. Becam, M. Dessertine, A. Vergnes, L. Aussel, B. Ezraty, Role of the multicopper oxidase CueO in copper homeostasis under anaerobic conditions in enterobacteria, Mol. Microbiol. (2025) 297–309, https://doi.org/10.1111/mmi.70010.
[28] N. Mano, A. de Poulpiquet, O2 reduction in enzymatic biofuel cells, Chem. Rev. 118 (2018) 2392–2468, https://doi.org/10.1021/acs.chemrev.7b00220.
[29] X. Xiao, H. Xia, R. Wu, L. Bai, L. Yan, E. Magner, S. Cosnier, E. Lojou, Z. Zhu, A. Liu, Tackling the challenges of enzymatic (bio)fuel cells, Chem. Rev. 119 (2019) 9509–9558, https://doi.org/10.1021/acs.chemrev.9b00115.
[30] T. Adachi, I. Mazurenko, N. Mano, Y. Kitazumi, K. Kataoka, K. Kano, K. Sowa, E. Lojou, Kinetic and thermodynamic analysis of Cu2+−dependent reductive inactivation in direct electron transfer-type bioelectrocatalysis by copper efflux oxidase, Electrochim. Acta 429 (2022) 140987, https://doi.org/10.1016/j.electacta.2022.140987.
[31] T. Adachi, T. Takei, T. Nishiyama, K. Kano, S. Yamashita, Roles of sixth bound copper in reductive inactivation of copper efflux oxidase, ChemRxiv (2025) 1–11.
[32] V. Saska, P. Santucci, A. de Poulpiquet, D. Gasparutto, U. Contaldo, I. Mazurenko, E. Lojou, Tuning O2 enzymatic reduction: roles of methionine-rich domains and electrochemical metalation of active centers, Bioelectrochemistry 166 (2025) 109051.

[33] S. Stoll, A. Schweiger, EasySpin, a comprehensive software package for spectral simulation and analysis in EPR, J. Magn. Reson. 178 (2006) 42–55. https://www.sciencedirect.com/science/article/pii/S1090780705002892.
[34] T.D. Goddard, C.C. Huang, E.C. Meng, E.F. Pettersen, G.S. Couch, J.H. Morris, T. E. Ferrin, UCSF ChimeraX: meeting modern challenges in visualization and analysis, Protein Sci. 27 (2018) 14–25.
[35] E.F. Pettersen, T.D. Goddard, C.C. Huang, E.C. Meng, G.S. Couch, T.I. Croll, J. H. Morris, T.E. Ferrin, UCSF ChimeraX: structure visualization for researchers, educators, and developers, Protein Sci. 30 (2021) 70–82.
[36] I. Olmeda, P. Casino, R.E. Collins, S. Callej, A.S. Soares, I. Pardo, Structural analysis and biochemical properties of laccase enzymes from two *Pediococcus* species, J. Microbiol. Biotechnol. 14 (3) (2021) 1026–1043.
[37] I. Olmeda, F. Paredes-Martínez, R. Sendra, P. Casino, I. Pardo, S. Ferrer, Biochemical and structural characterization of a novel psychrophilic Laccase (multicopper oxidase) discovered from Oenococcus oeni 229 (ENOLAB 4002), Int. J. Mol. Sci. 25 (2024).
[38] R. Gasco, R. Sendra, I. Olmeda, F. Paredes-Martínez, S. Ferrer, I. Pardo, P. Casino, Laccases from lactic acid bacteria show cuprous oxidase activity and capture Cu(II) and Ag(I) ions, Protein Sci. (2026) 1–17, https://doi.org/10.1002/pro.70385.
[39] V.P. Hitaishi, R. Clément, L. Quattrocchi, P. Parent, D. Duché, L. Zuily, M. Ilbert, E. Lojou, I. Mazurenko, Interplay between orientation at electrodes and copper activation of Thermus thermophilus Laccase for O2 reduction, J. Am. Chem. Soc. 142 (2020) 1394–1405.
[40] R. Clément, X. Wang, F. Biaso, M. Ilbert, I. Mazurenko, E. Lojou, Mutations in the coordination spheres of T1 cu affect Cu2+−activation of the laccase from Thermus thermophilus, Biochimie 182 (2021) 228–237.
[41] P. Stolle, B. Hou, T. Brüser, The tat substrate CueO is transported in an incomplete folding state, J. Biol. Chem. 291 (2015) 13520–13528.
[42] T.R. Young, A.G. Wedd, Z. Xiao, Evaluation of Cu(I) binding to the E2 domain of the amyloid precursor protein – a lesson in quantification of metal binding to proteins via ligand competition, Metallomics 10 (2018) 108–119, https://doi.org/10.1039/C7MT00291B.
[43] Z. Xiao, F. Loughlin, G.N. George, G.J. Howlett, A.G. Wedd, C-terminal domain of the membrane copper transporter Ctr1 from Saccharomyces cerevisiae binds four Cu(I) ions as a cuprous-thiolate polynuclear cluster: sub-femtomolar Cu(I) affinity of three proteins involved in copper trafficking, J. Am. Chem. Soc. 126 (2004) 3081–3090.
[44] Z. Xiao, P.S. Donnelly, M. Zimmermann, A.G. Wedd, Transfer of copper between bis(thiosemicarbazone) ligands and intracellular copper-binding proteins. Insights into mechanisms of copper uptake and hypoxia selectivity, Inorg. Chem. 47 (2008) 4338–4347.
[45] P. Bagchi, M.T. Morgan, J. Bacsa, C.J. Fahrni, Robust affinity standards for Cu (I) biochemistry, J. Am. Chem. Soc. 135 (2013) 18549–18559.
[46] Z. Xiao, J. Brose, S. Schimo, S.M. Ackland, S. La Fontaine, A.G. Wedd, Unification of the copper(I) binding affinities of the metallo-chaperones Atx1, Atox1, and related proteins: detection probes and affinity standards, J. Biol. Chem. 286 (2011) 11047–11055.
[47] K.Y. Djoko, L.X. Chong, A.G. Wedd, Z. Xiao, Reaction mechanisms of the multicopper oxidase CueO from Escherichia coli support its functional role as a cuprous oxidase, J. Am. Chem. Soc. 132 (2010) 2005–2015.
[48] J.I. Badillo-Gómez, I. Suarez-Antuña, I. Mazurenko, F. Biaso, J. Pécaut, E. Lojou, P. Delangle, S. Hostachy, Biomimetic pseudopeptides to decipher the interplay between Cu and methionine-rich domains in proteins, Chem. Eur. J. 31 (2025), https://doi.org/10.1002/chem.202403896.
[49] D.L. Huffman, T.V.O. Halloran, Energetics of copper trafficking between the Atx1 metallochaperone and the intracellular copper transporter, Ccc2*, J. Biol. Chem. 275 (2000) 18611–18614, https://doi.org/10.1074/jbc.C000172200.
[50] D.S. Yuan, A. Dancis, R.D. Klausner, Restriction of copper export in Saccharomyces cerevisiae to a late Golgi or post-Golgi compartment in the secretory pathway *, J. Biol. Chem. 272 (1997) 25787–25793, https://doi.org/10.1074/jbc.272.41.25787.
[51] N.E. Hellman, S. Kono, G.M. Mancini, A.J. Hoogeboom, G.J. de Jong, J.D. Gitlin, Mechanisms of copper incorporation into human ceruloplasmin, J. Biol. Chem. 277 (2002) 46632–46638, https://doi.org/10.1074/jbc.M206246200.
[52] N. Maio, F. Polticelli, G. De Francesco, G. Rizzo, M. Carmela, G. Musci, Role of external loops of human ceruloplasmin in copper loading by ATP7B and Ccc2p, J. Biol. Chem. 285 (2010) 20507–20513, https://doi.org/10.1074/jbc.M109.090027.
[53] N. Barnes, R. Tsivkovskii, N. Tsivkovskaia, S. Lutsenko, The copper-transporting ATPases, Menkes and Wilson disease proteins, have distinct roles in adult and developing cerebellum, J. Biol. Chem. 280 (2005) 9640–9645, https://doi.org/10.1074/jbc.M413840200.
[54] M. Solioz, Copper homeostasis in gram-negative bacteria, in: Copp. Bact, Springer, 2018, pp. 49–80.
[55] F.Q. Schafer, G.R. Buettner, Redox environment of the cell as viewed through the redox state of the glutathione disulfide/glutathione couple, Free Radic. Biol. Med. 30 (2001) 1191–1212.
[56] Y. Li, J. Hugenholtz, T. Abee, D. Molenaar, Glutathione protects Lactococcus lactis against oxidative stress, Appl. Environ. Microbiol. 69 (2003) 5739–5745.
[57] L. Zuily, N. Lahrach, E. Falcone, M. Bouraguba, V. Lebrun, E. Lojou, M. Giudici-Orticoni, P. Faller, M. Ilbert, Ligands as a tool to tune the toxicity of Cu on bacteria: from boosting to silencing, in: Copp. Bioinorg. Chem., 2023, pp. 1–44.
[58] A. Andrei, Y. Öztürk, B. Khalfaoui-Hassani, J. Rauch, D. Marckmann, P.I. Trasnea, F. Daldal, H.G. Koch, Cu homeostasis in bacteria: the ins and outs, Membranes (Basel) 10 (2020) 1–45.
[59] V. Vassiliev, Z.L. Harris, P. Zatta, Ceruloplasmin in neurodegenerative diseases, Brain Res. Rev. 49 (2005) 633–640.
[60] V.V. Orzheshkovskyi, M.A. Trishchynska, Ceruloplasmin: its role in the physiological and pathological processes, Neurophysiology 51 (2019) 141–149.
[61] G. Vashchenko, R.T.A. MacGillivray, Multi-copper oxidases and human iron metabolism, Nutrients 5 (2013) 2289–2313.